Exploring hardness enhancement in superhard tungsten tetraboride-based solid solutions using radial X-ray diffraction

Miao Xie, Reza Mohammadi, Christopher L. Turner, Richard B. Kaner, Abby Kavner, and Sarah H. Tolbert

Citation: Appl. Phys. Lett. **107**, 041903 (2015); doi: 10.1063/1.4927596
View online: http://dx.doi.org/10.1063/1.4927596
View Table of Contents: http://aip.scitation.org/toc/apl/107/4
Published by the American Institute of Physics

Exploring hardness enhancement in superhard tungsten tetraboride-based solid solutions using radial X-ray diffraction

Miao Xie,[1] Reza Mohammadi,[1,2,a)] Christopher L. Turner,[1] Richard B. Kaner,[1,2,3,b)] Abby Kavner,[4,b)] and Sarah H. Tolbert[1,2,3,b)]
[1]*Department of Chemistry and Biochemistry, UCLA, Los Angeles, California 90095, USA*
[2]*Department of Materials Science and Engineering, UCLA, Los Angeles, California 90095, USA*
[3]*The California NanoSystems Institute (CNSI), UCLA, Los Angeles, California 90095, USA*
[4]*Department of Earth, Planetary, and Space Sciences, UCLA, Los Angeles, California 90095, USA*

(Received 17 March 2015; accepted 17 July 2015; published online 29 July 2015)

In this work, we explore the hardening mechanisms in WB_4-based solid solutions upon addition of Ta, Mn, and Cr using *in situ* radial X-ray diffraction techniques under non-hydrostatic pressure. By examining the lattice-supported differential strain, we provide insights into the mechanism for hardness increase in binary solid solutions at low dopant concentrations. Speculations on the combined effects of electronic structure and atomic size in ternary WB_4 solid solutions containing Ta with Mn or Cr are also included to understand the extremely high hardness of these materials.
 [http://dx.doi.org/10.1063/1.4927596]

The development of superhard materials is driven by applications ranging from cutting and forming tools to wear-resistant coatings. While most superhard materials are made from combinations of first-row elements (e.g., diamond, cubic boron nitride), an alternative and very effective approach is to introducing light p-block elements into late transition metals.[1] Examples of such materials include superhard transition metal borides.[1–6] With a Vickers hardness above 40 GPa,[3] relatively easy synthesis at ambient pressure,[3,5] excellent electrical conductivity,[7] high bulk modulus (344–369 GPa),[3,8–10] and high shear modulus (223–273 GPa),[9–12] rhenium diboride (ReB_2) is a prime example of this family. Since the addition of two boron atoms per transition metal induces covalent bonding that strengthens the lattice and converts comparatively soft elemental Re, into superhard ReB_2, one might expect that higher concentrations of boron would continue increasing the hardness. This idea led to highly incompressible and superhard tungsten tetraboride (WB_4), which contains twice as many boron atoms per metal as the diborides.[4,6,8]

Recently, our group has unambiguously solved the structure of WB_4 by combined refinement of X-ray powder, X-ray single crystal, and neutron time-of-flight power diffraction data.[13] The analysis indicates that the crystal structure of WB_4 consists of alternating hexagonal layers of boron and tungsten with some tungsten sites showing only partial occupancy. Boron trimers sit on those unoccupied sites; the boron atoms are distributed around the unoccupied W sites and combine with boron in the hexagonal layers to form distorted cuboctahedra cages. The rigid boron cages along the *c*-direction help WB_4 not only resists hydrostatic compression (high bulk modulus of 326–339 GPa)[4,8,14] but also support a high differential stress of 15.8 GPa at a confining pressure of 48.5 GPa[15] and show a Vickers hardness ~43 GPa (0.49 N applied load).[4,16]

The WB_4 structure is able to accommodate dopants with varying valence-electron count and atomic size. This flexibility allows the hardness of WB_4 to be tuned by adding other transition metals including tantalum (Ta), manganese (Mn), and chromium (Cr).[6] We have recently shown that Vickers hardnesses of 52.8 ± 0.6, 53.7 ± 0.5, and 53.5 ± 0.5 GPa could be achieved under an applied load of 0.49 N, when 2.0, 4.0, and 10.0 at. % Ta, Mn, and Cr, respectively, were added to WB_4 on a metals basis.[6] Interestingly, in WB_4-Mn solid solutions, the hardness data showed two nearly equivalent peaks with the addition of 4.0 and 10.0 at. % Mn. Table I summarizes the maximum low and high load hardness values obtained for various WB_4 solid solutions. Also included in the table are two optimized ternary compositions with hardness values of 55.8 ± 0.5 and 57.3 ± 0.5 GPa (at 0.49 N applied load) for the combinations $W_{0.94}Ta_{0.02}Mn_{0.04}B_4$ and $W_{0.93}Ta_{0.02}Cr_{0.05}B_4$, respectively.

Our goal here is to use high-pressure studies to understand the mechanism for these increases in hardness. For example, solid-solution hardening, which occurs when atoms with different sizes reside in equivalent lattice sites, is well

TABLE I. Vickers microindentation hardness for selected WB_4 solid solutions. The table summarizes data obtained at the highest and lowest indentation loads measured. All reported errors are standard deviations of the mean, calculated across multiple indentations for a given sample composition.

	Applied load (N)	
Compound	0.49	4.9
WB_4	43.3 ± 0.6	28.1 ± 0.4
$W_{0.94}Ta_{0.02}B_4$	52.8 ± 0.6	33.5 ± 0.3
$W_{0.96}Mn_{0.04}B_4$	53.7 ± 0.5	31.7 ± 0.2
$W_{0.90}Mn_{0.10}B_4$	53.9 ± 0.5	31.4 ± 0.3
$W_{0.90}Cr_{0.10}B_4$	53.5 ± 0.5	32.4 ± 0.4
$W_{0.94}Ta_{0.02}Mn_{0.04}B_4$	55.8 ± 0.5	30.9 ± 0.2
$W_{0.93}Ta_{0.02}Cr_{0.05}B_4$	57.3 ± 0.5	31.7 ± 0.2

[a)]Present address: Department of Mechanical and Nuclear Engineering, School of Engineering, Virginia Commonwealth University, Richmond, Virginia 23284-3067, USA.
[b)]Authors to whom correspondence should be addressed. Electronic addresses: kaner@chem.ucla.edu; akavner@ucla.edu; and tolbert@chem.ucla.edu

established in mixed materials,[17] but it is not commonly observed in solid solutions containing as few dopant atoms as those examined here. Moreover, the two hardness maxima observed in Mn-doped WB_4 suggest that multiple hardening mechanisms are at work. In our previous work, this solid-solution hardening was attributed to electronic structure changes, including the distribution of rigid boron cages, caused by differences in valence electron count between W, Ta, Mn, and Cr, together with atomic-size mismatch effects (Ta = 1.49 Å, Mn = 1.32 Å, Cr = 1.30 Å, and W = 1.41 Å).[6] Simple hardness tests cannot distinguish between these various mechanisms, however.

To elucidate the hardening mechanisms in these WB_4-based solid solutions, we have employed non-hydrostatic high-pressure diffraction (radial X-ray diffraction, RXRD),[18] using beamline 12.2.2 at the Advanced Light Source (LBNL). By comparing the lattice-supported differential stress/strain across materials compositions and lattice planes, we can separate intrinsic bonding effects from composite effects. We can also directly compare bonding changes in a lattice specific manner and relate those to the WB_4 crystal structure.

Polycrystalline samples were synthesized by arc melting from the pure elements.[6] Ingots were then ground to fine powders in a Plattner's-style hardened tool-steel mortar and pestle set (Humboldt Mfg., Model H-17270) and passed through a No. 850 mesh sieve (<10 μm). Trace element impurities introduced during grinding (e.g., iron) were removed by washing 3× in 1M HCl. Final sample purity was confirmed by XRD and energy dispersive spectroscopy (EDS). A scanning electron micrograph of a ground sample is shown in Figure S1.[19] A diamond anvil cell (DAC) equipped with 300 μm diamond culets was used for high-pressure measurement in combination with an X-ray transparent boron/epoxy gasket.[20] Pre-compressed 40-μm diameter metal-boride samples and a 30-μm diameter platinum foil (used as a pressure standard) were then deposited in the 70-μm-diameter × 40-μm-thick gasket hole. For diffraction measurements, a 10 × 10 μm X-ray beam was directed onto the sample perpendicular to the loading axis through the gasket. The sample to detector distance, detector tile, and pixel-size ratio were calibrated using LaB_6. Angle-dispersive diffraction patterns were collected at room temperature and converted from elliptical to rectangular coordinates using FIT2D.[21] The resulting "caked" patterns, graphed as azimuthal angle η versus diffraction angles 2θ, were then analyzed using Igor Pro (WaveMetrics, Inc.). Peak positions were individually determined for six easily resolvable diffraction peaks (101, 002, 110, 201, 112, and 103).

Because of the non-hydrostatic stress, the measured d spacings ($d_m(hkl)$) depend on the angle φ between the diffracting plane normal and the load axis, expressed as $d_m(hkl) = d_p(hkl)[1 + (1 - 3\cos^2\varphi)Q(hkl)$.[22,23] Here, $d_p(hkl)$ is the d spacing due to the hydrostatic component of the strain. The angle φ is calculated from $\cos\varphi = (\cos\theta)(\cos\eta)$. The lattice strain is given by $Q(hkl) = \frac{t}{3}\left[\frac{\alpha}{2G_R(hkl)} + \frac{1-\alpha}{2G_V}\right]$. $G_R(hkl)$ and G_V are the shear moduli of the aggregate under the Reuss (iso-stress) and Voigt (isostrain) approximations, respectively, and $0 \le \alpha \le 1$. According to the von Mises yield criterion, $t = \sigma_3 - \sigma_1 \le 2\tau = \sigma_y$, where τ is the shear strength and σ_y is the yield strength. The maximum elastically supported differential stress (t) thus provides a lower-bound estimate of the material's yield strength. In elastically anisotropic materials like WB_4 under Reuss conditions, t for each lattice plane can be estimated using $t(hkl) = 6G(hkl)Q(hkl)$.[24,25]

Figure 1 shows caked diffraction patterns for the hardest WB_4 solid solution, $W_{0.93}Ta_{0.02}Cr_{0.05}B_4$. At low pressure (1.3 GPa), the diffraction lines are almost straight (constant d spacing) due to the small non-hydrostatic stress (Fig. 1(a)). Small variations in the positions of the diffraction peaks are observed in the Pt pattern, however, indicating that $W_{0.93}Ta_{0.02}Cr_{0.05}B_4$ supports a higher stress than Pt. As compression increases, the difference between $2\theta_{max}$ (maximum stress direction, $\varphi = 0°$) and $2\theta_{min}$ (minimum stress direction, $\varphi = 90°$ and $-90°$) becomes larger (Fig. 1(b)). This can be seen from the sinusoidal variations of the diffraction lines, which are associated with lattice-supported strains.

Because lattice-dependent elasticity information is not yet available for WB_4-based solid solutions or for pure WB_4 with the experimentally determined crystal structure,[13] we consider the ratio $t(hkl)/G(hkl)$, which reflects the differential strain elastically supported by the lattice planes under an imposed differential stress.[26–28] Because variations in $G(hkl)$ across solid solutions are likely to be modest, general trends in $t(hkl)/G(hkl)$ should be good qualitative indicators of trends in $t(hkl)$, though small quantitative differences are likely.[29] The $t(hkl)/G(hkl)$ ratio can be calculated directly from the lattice strain parameter $Q(hkl)$ for each diffraction peak. Figure 2 shows $t(hkl)/G(hkl)$ for representative planes of pure WB_4 and its binary solid solutions as a function of pressure. Up to a pressure of 20 GPa, all $t(hkl)/G(hkl)$ ratios increase linearly, indicating elastic deformation. As the pressure increases above 20 GPa, the increase in $t(hkl)/G(hkl)$ slows and levels off at 35–40 GPa, presumably indicating the onset of plastic deformation.

Overall, $t(hkl)/G(hkl)$ ratios for all solid solutions exhibit trends similar to pure WB_4; the (002) planes support the

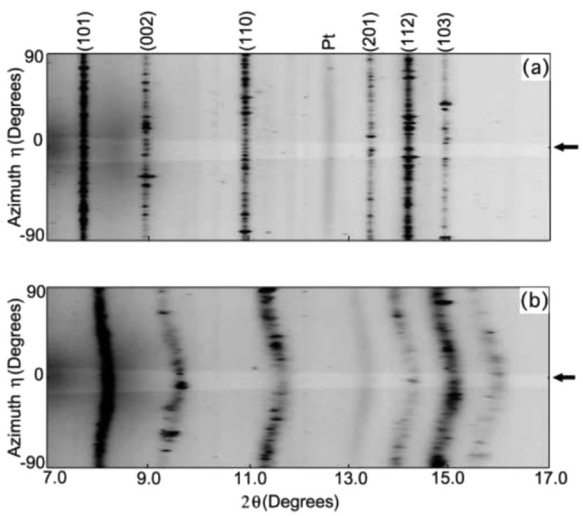

FIG. 1. Caked diffraction patterns for the hardest WB_4 solid solution, $W_{0.93}Ta_{0.02}Cr_{0.05}B_4$, at a pressure of 1.3 (a) and 56.5 GPa (b) in the diamond anvil cell. The images show the diffraction as a function of the Bragg angle 2θ and the azimuth angle η on the image plate. The compression directions are indicated by the dark arrows.

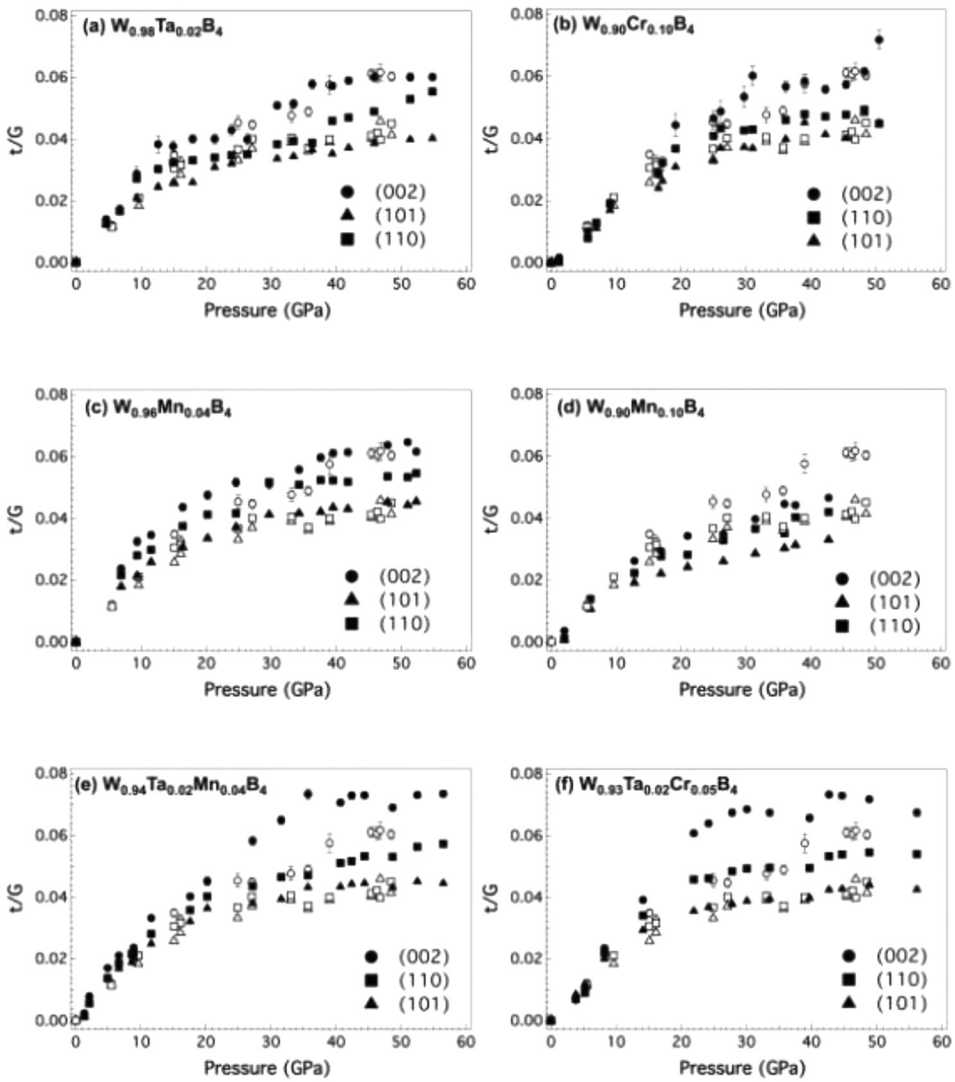

FIG. 2. The ratio of differential stress to shear modulus *t(hkl)/G(hkl)* upon addition of 2.0 at. % Ta (a), 10.0 at. % Cr (b), 4.0 at. % Mn (c), and 10.0 at. % Mn (d) to WB_4, and the two hardest ternary solid solutions, $W_{0.94}Ta_{0.02}Mn_{0.04}B_4$ (e) and $W_{0.97}Ta_{0.02}Cr_{0.05}B_4$ (f). In all cases, solid symbols correspond to the solid-solution data, and open symbols correspond to pure WB_4, which are included for comparison. Error bars, when not shown, are smaller than the symbol.

highest differential strain, followed by the (110) and (101) planes. While we have no experimental data on the positions of dopant atoms in the lattice, this suggests that they simply substitute for tungsten in metal sites. The strain anisotropy can likely be attributed to the three-dimensional covalently bonded structure of WB_4. The tungsten and boron layers in the *a-b* plane, which appear to be slip planes in many hard metal borides,[30,31] are held together upon pressurizing by rigid boron cages, preventing the layers from shearing. As a result, the (002) planes, parallel to the layers of boron and tungsten atoms, are able to withstand higher differential strains than the (110) planes, which are perpendicular to the layers. This contrasts to ReB_2, another hard transition metal boride, where symmetry-related (004) planes are not cross-linked by boron cages and support the least differential strain.[15]

When 2.0 at. % Ta is added to WB_4, the resulting solid solution shows a slight increase of *t(hkl)/G(hkl)* in the (002) and (110) planes compared to pure WB_4; no changes in the (101) planes were observed (Fig. 2(a)). Similar small changes are observed upon addition of 10.0 at. % Cr to WB_4 (Fig. 2(b)). By contrast, the addition of 4.0 at. % Mn on a metals basis significantly raises *t(hkl)/G(hkl)* in all studied planes (Fig. 2(c)). However, when a higher concentration (10.0 at. % Mn) was used, *t(hkl)/G(hkl)* showed a universal decrease compared to both the 4.0 at. % Mn sample and to pure WB_4 (Fig. 2(d)). These two solid solutions show nearly identical hardness values (Table I), but these data suggest fundamentally different hardening mechanisms.

Mechanisms to increase *t(hkl)/G(hkl)* include changes in electronic structure and bonding, including changes in the spatial distribution of boron cages and changes in accessible slip systems due to size mismatch of dopant atoms. Ta and Mn have one less and one more valence electron than W, respectively; and so we might expect electronic structure changes in solid their solutions. Valence electron concentration (VEC) changes up to 0.3% result from the dopant levels used here. Optimized VEC should result in maximized bond covalency. This effect has been previously observed in transition metal carbide solid solutions such as $Ti_xNb_{1-x}C$ and $Zr_xNb_{1-x}C$.[32] This hypothesis is also supported by first-principle calculations by several groups, who found that vacancies in various WB_x-type structures are favored electronically by a reduction of the Fermi level.[33,34] Thus, it is reasonable that optimizing the VEC could result in more fully populated bonding states or less populated antibonding states, both of which could decrease the Fermi level and improve the capability of lattice planes to support the deviatoric stress.

Another explanation for increases in *t(hkl)/G(hkl)* is atomic size effects influencing available slip systems. Ta is

similar in size to W. Previous work on solid solutions of OsB_2 and RuB_2 (which also have similar sizes) showed no improvements in hardening,[35] so it is reasonable to assume few size effects from adding Ta to W. Observed *t(hkl)/G(hkl)* changes in the 2.0 at. % Ta sample should thus be dominated by electronic structure effects. Mn, however, is much smaller than W, so size effects are expected. Indeed, significantly larger *t(hkl)/G(hkl)* changes are observed for 4.0 at. % Mn in WB_4 compared to 2.0 at. % Ta in WB_4. The effects cannot be purely size-based, however, because when 10.0 at. % Mn is used, the solid solution showed a lower *t(hkl)/G(hkl)* ratio (Figs. 2(c) and 2(d)). This result strongly suggests that 10.0 at. % Mn in WB_4 exceeds the optimal VEC, and this material supports a lower differential strain primarily for electronic structure reasons. Pure size mismatch effects should only improve as the Mn concentration increases. These results further indicate that the high hardness observed for the 10.0 at. % Mn samples (Table I) likely arises from extrinsic effects such as the appearance of a second phase. The presence of diffraction from MnB_4 at higher Mn concentrations confirms this notion.[6] The ability to distinguish between intrinsic and extrinsic hardening effects is a powerful aspect of these radial diffraction studies.

For the case of the WB_4-Cr system, again only small changes in *t(hkl)/G(hkl)* are observed. Both Cr and W are group VI elements, so the VEC remains constant regardless of dopant concentration and no electronic structure change are expected in Cr doped WB_4. Cr is much smaller than W, however (similar to Mn). Figure 2(b) shows that adding 10% Cr to WB_4 increases in the plateau *t/G* value for the (110) lattice plane and slightly decrease the plateau pressure for the (002) plane. The small magnitude of the effect in Cr-WB_4 compared to 4 at. % Mn-WB_4, however, emphasizes the potential for synergy between size and electronic structure effects.

To further explore this synergy between size and electronic effects, we examined the combined effects of size and electron count in ternary alloys. Here, we report *t(hkl)/G(hkl)* for two of the hardest ternary solid solutions that we were able to produce: $W_{0.94}Ta_{0.02}Mn_{0.04}B_4$ and $W_{0.97}Ta_{0.02}Cr_{0.05}B_4$. Considerable increases of *t(hkl)/G(hkl)* are observed when Ta and either Mn or Cr are simultaneously added to WB_4 (Figures 2(e) and 2(f)). $W_{0.94}Ta_{0.02}Mn_{0.04}B_4$ shows an ~18% increase in the plateau *t(hkl)/G(hkl)* value for the (002) planes and a 29% increase in the plateau value of the (110) planes. Similarly, large increases are observed in $W_{0.97}Ta_{0.02}Cr_{0.05}B_4$. Interestingly, the (101) planes in both samples show less change in *t(hkl)*/G(hkl). We note that both samples have a net change in VEC when electronic contribution from both atoms is considered, and both systems contain a reasonable concentration of very small atoms.

Complementary evidence of structural synergy in ternary solid solutions is found in our previously measured lattice constants.[6] Ternary systems show consistently slightly smaller lattice constants than corresponding binaries. This could be due to non-random metal substitution at distinct lattice sites or to increased covalency.[13] Overall, these results reemphasize the key conclusion of this work that hardness in WB_4 based solutions can be best optimized by combining size-mismatch and VEC changes.

In conclusion, we have conducted non-hydrostatic high pressure diffraction studies on WB_4-based solid solutions containing Ta, Mn, and Cr. By examining the lattice-supported differential strain across compositions, we can differentiate between hardening mechanisms and expand on traditional hardness measurements. This is thus a step forward in understanding these low-cost, easily manufactured superhard transition metal borides, and it provides a roadmap for future materials selection and the design of next-generation superhard materials.

The authors thank A. T. Lech for providing structural information; M. M. Armentrout for assistance with data analysis; B. Chen, J. Y. Yan, A. MacDowell, and M. T. Yeung for experimental support; and Professor H.-R. Wenk, E. A. Alarcon, Professor T. Duffy, and C. V. Stan for the use of their equipment. This work was funded by the National Science Foundation under Grant Nos. DMR-1106364 and 1506860 (S.H.T. and R.B.K.) and by the NNSA through a Carnegie/DOE alliance center Grant No. DE-NA-00006 (A.K.). Portions of this work were performed at the Advanced Light Source (LBNL). The Advanced Light Source is supported by the Director, Office of Science, Office of Basic Energy Sciences, of the U.S. Department of Energy under Contract No. DE-AC02-05CH11231. This research was partially supported by COMPRES, the Consortium for Materials Properties Research in Earth Sciences under NSF Cooperative Agreement No. EAR 11-57758.

[1]R. B. Kaner, J. J. Gilman, and S. H. Tolbert, Science **308**, 1268 (2005).
[2]R. Mohammadi and R. B. Kaner, "Superhard materials," in *Encyclopedia of Inorganic and Bioinorganic Chemistry*, edited by R. A. Scott (John Wiley, Chichester, 2012).
[3]H.-Y. Chung, M. B. Weinberger, J. B. Levine, A. Kavner, J.-M. Yang, S. H. Tolbert, and R. B. Kaner, Science **316**, 436 (2007).
[4]R. Mohammadi, A. T. Lech, M. Xie, B. E. Weaver, M. T. Yeung, S. H. Tolbert, and R. B. Kaner, Proc. Natl. Acad. Sci. U.S.A. **108**, 10958 (2011).
[5]J. B. Levine, S. H. Tolbert, and R. B. Kaner, Adv. Funct. Mater. **19**, 3519 (2009).
[6]R. Mohammadi, M. Xie, A. T. Lech, C. L. Turner, A. Kavner, S. H. Tolbert, and R. B. Kaner, J. Am. Chem. Soc. **134**, 20660 (2012).
[7]J. B. Levine, S. L. Nguyen, H. I. Rasool, J. A. Wright, S. E. Brown, and R. B. Kaner, J. Am. Chem. Soc. **130**, 16953 (2008).
[8]M. Xie, R. Mohammadi, Z. Mao, M. M. Armentrout, A. Kavner, R. B. Kaner, and S. H. Tolbert, Phys. Rev. B **85**, 064118 (2012).
[9]M. R. Koehler, V. Keppens, B. C. Sales, R. Jin, and D. Mandrus, J. Phys. D **42**, 095414 (2009).
[10]J. B. Levine, J. B. Betts, J. D. Garrett, S. Q. Guo, J. T. Eng, A. Migliori, and R. B. Kaner, Acta Mater. **58**, 1530 (2010).
[11]S. N. Tkachev, J. B. Levine, A. Kisliuk, A. P. Sokolov, S. Guo, J. T. Eng, and R. B. Kaner, Adv. Mater. **21**, 4284 (2009).
[12]Y. Suzuki, J. B. Levine, A. Migliori, J. D. Garrett, R. B. Kaner, V. R. Fanelli, and J. B. Betts, J. Acoust. Soc. Am. **127**, 2797 (2010).
[13]A. T. Lech, C. L. Turner, R. Mohammadi, S. H. Tolbert, and R. B. Kaner, Proc. Natl. Acad. Sci. U.S.A. **112**, 3223 (2015).
[14]L. Xiong, J. Liu, L. G. Bai, Y. C. Li, C. L. Lin, D. W. He, F. Peng, and J. F. Lin, J. Appl. Phys. **113**, 033507 (2013).
[15]M. Xie, R. Mohammadi, C. L. Turner, R. B. Kaner, A. Kavner, and S. H. Tolbert, Phys. Rev. B **90**, 104104 (2014).
[16]Q. Gu, G. Krauss, and W. Steurer, Adv. Mater. **20**, 3620 (2008).
[17]G. E. Dieter, *Mechanical Metallurgy*, 3rd ed. (McGraw-Hill Book Co., New York, 1986).
[18]H. K. Mao, J. F. Shu, G. Y. Shen, R. J. Hemley, B. S. Li, and A. K. Singh, Nature **396**, 741 (1998).
[19]See supplementary material at http://dx.doi.org/10.1063/1.4927596 for additional materials characterization.
[20]S. Merkel and T. Yagi, Rev. Sci. Instrum. **76**, 046109 (2005).

[21]A. P. Hammersley, S. O. Svensson, M. Hanfland, A. N. Fitch, and D. Hausermann, High Pressure Res. **14**, 235 (1996).
[22]A. K. Singh, J. Appl. Phys. **73**, 4278 (1993).
[23]A. K. Singh, C. Balasingh, H. K. Mao, R. J. Hemley, and J. F. Shu, J. Appl. Phys. **83**, 7567 (1998).
[24]T. Uchida, Y. B. Wang, M. L. Rivers, and S. R. Sutton, Earth Planet. Sci. Lett. **226**, 117 (2004).
[25]G. M. Amulele, M. H. Manghnani, and M. Somayazulu, J. Appl. Phys. **99**, 023522 (2006).
[26]A. Kavner, M. B. Weinberger, A. Shahar, R. W. Cumberland, J. B. Levine, R. B. Kaner, and S. H. Tolbert, J. Appl. Phys. **112**, 013526 (2012).
[27]D. W. He, S. R. Shieh, and T. S. Duffy, Phys. Rev. B **70**, 184121 (2004).
[28]T. S. Duffy, AIP Conf. Proc. **955**, 639 (2007).
[29]M. B. Kanoun, P. Hermet, and S. Goumri-Said, J. Phys. Chem. C **116**, 11746 (2012).
[30]P. Lazar, X.-Q. Chen, and R. Podloucky, Phys. Rev. B **80**, 012103 (2009).
[31]C. Zang, H. Sun, and C. Chen, Phys. Rev. B **86**, 180101 (2012).
[32]S. H. Jhi, J. Ihm, S. G. Louie, and M. L. Cohen, Nature **399**, 132 (1999).
[33]Y. C. Liang, X. Yuan, and W. Q. Zhang, Phys. Rev. B **83**, 220102 (2011).
[34]H. Gou, Z. Li, L.-M. Wang, J. Lian, and Y. Wang, AIP Adv. **2**, 012171 (2012).
[35]M. B. Weinberger, J. B. Levine, H.-Y. Chung, R. W. Cumberland, H. I. Rasool, J.-M. Yang, R. B. Kaner, and S. H. Tolbert, Chem. Mater. **21**, 1915 (2009).